Available online at www.sciencedirect.com
SCIENCE DIRECT®
Journal of Solid State Chemistry 178 (2005) 172–179
JOURNAL OF SOLID STATE CHEMISTRY
www.elsevier.com/locate/jssc

Crystal structure, conductivity and reversible water uptake of new layered potassium antimonates $K_xL_{(1+x)/3}Sb_{(2-x)/3}O_2$ ($L = Ni^{2+}$, Mg^{2+}, Co^{2+})

O.A. Smirnova[a,b,*], V.B. Nalbandyan[b], M. Avdeev[a], L.I. Medvedeva[b], B.S. Medvedev[b], V.V. Kharton[a], F.M.B. Marques[a]

[a]*Department of Ceramics and Glass Engineering, CICECO, University of Aveiro, 3810-193 Aveiro, Portugal*
[b]*Chemistry Faculty, Rostov State University, Zorge 7, 344090 Rostov-on-Don, Russia*

Received 9 January 2004; received in revised form 13 July 2004; accepted 20 July 2004

Abstract

Novel mixed potassium antimonates $K_{0.59}Mg_{0.53}Sb_{0.47}O_2$, $K_{0.5}Ni_{0.5}Sb_{0.5}O_2$, $K_{0.5}Co_{0.5}Sb_{0.5}O_2$ (rhombohedral P3-type structure), $K_{0.56}Ni_{0.52}Sb_{0.48}O_2$ and $K_{0.86}Co_{0.62}Sb_{0.38}O_2$ (hexagonal P2 type) have layered structures based on brucite-like $(L,Sb)O_{6/3}$ sheets of edge-shared octahedra and interlayer K^+ cations in trigonal prismatic coordination. The preference to form P2 and P3 structures rather than closely related O3 type is dictated by the large radius of K^+ and the value of unit cell parameter **a**, restricted by average size of the cations randomly distributed in the octahedral sites within $(L,Sb)O_{6/3}$ layer. The new phases reversibly absorb atmospheric moisture leading to the formation of hydrates with ca. 11% larger interlayer distances. The impedance spectroscopy of P2-type $K_{0.56}Ni_{0.52}Sb_{0.48}O_2$ and P3-type $K_{0.59}Mg_{0.53}Sb_{0.47}O_2$ ceramics shows relatively high ionic conductivity, presumably due to potassium cationic transport, with activation energies of 35 ± 2 and 33 ± 1 kJ/mol, respectively. At 573 K, the conductivity values are 0.016 S/cm for $K_{0.56}Ni_{0.52}Sb_{0.48}O_2$ and 0.021 S/cm for $K_{0.59}Mg_{0.53}Sb_{0.47}O_2$. Interaction with water vapor leads to increasing total conductivity.

Keywords: Layered potassium antimonates; X-ray diffraction; Rietveld refinement; Ionic conductivity; Impedance spectroscopy; Water absorption

1. Introduction

Materials with fast alkali cation transport receive great attention for electrochemical applications, including gas sensors, ion-selective electrodes and rechargeable batteries [1–4]. The oxide family of general formula $A_x(L,M)O_2$, forming a variety of crystal structures based upon brucite-like $(L,M)O_{6/3}$ sheets of edge-shared metal–oxygen octahedra, is well known for A^+ cation transport properties. For $A^+ = Na^+$ or K^+, the most common structures belong to the so-called P2, P3 and O3 types, where the letters show coordination of an interlayer alkali cation (P—trigonal prismatic, O—octahedral) and the digits indicate the number of layers in a hexagonal unit cell [5]. Delmas et al. [6,7] described two series of potassium ion conductors with such layered structures, namely $K_x(L_xM_{1-x})O_2$ (L = In, Sc; M = Zr, Hf, Sn, Pb) and $K_x(L_{x/2}Sn_{1-x/2})O_2$ (L = Mg, Ca, Zn). Of these, P2-type $K_{0.72}(In_{0.72}Sn_{0.28})O_2$ exhibits maximum conductivity values, higher than those of potassium beta alumina. Later, a number of cation-conducting P2-type titanates $Na_x(L_yTi_{1-y})O_2$ (L = Ni, Co, Cr, Li) were described [8–16]. Alkali cation transport in these compounds is favored by wide rectangular bottlenecks between prismatic cation sites and by low ionicity of (L,M)–O bonds leading to high ionicity of the O–K (or O–Na) bonds [6–7,17].

*Corresponding author. Department of Ceramics and Glass Engineering, CICECO, University of Aveiro, 3810-193 Aveiro, Portugal. Fax: +351 234 425300.
E-mail address: osmirnova@cv.ua.pt (O.A. Smirnova).

0022-4596/$ - see front matter © 2004 Elsevier Inc. All rights reserved.
doi:10.1016/j.jssc.2004.07.059

Formation of analogous layered phases may be expected in ternary oxide systems containing Sb^{5+}, which has an ionic radius close to that of Ti^{4+} and a higher electronegativity compared to titanium or tin. However, in the systems Na_2O–LO_x–Sb_2O_5 ($L = Fe^{3+}$, Mg^{2+}, Co^{2+}, Ni^{2+}), only O3-type phases were found [18]. The aim of the present work was to investigate the compound formation in the K-containing quasi-ternary oxide systems K_2O–LO–Sb_2O_5 ($L = Ni^{2+}$, Mg^{2+}, Co^{2+}, Cu^{2+}, Zn^{2+}) and to characterize new ternary oxides.

2. Experimental

The powder samples were prepared by a conventional solid-state reaction technique using K_2CO_3, $Sb_2O_5 \cdot x$-H_2O, NiO, $Ni(CH_3COO)_2 \cdot xH_2O$, nickel carbonate, magnesium hydroxide carbonate, zinc hydroxide carbonate, copper hydroxide carbonate, and cobalt carbonate as starting materials. Potassium carbonate was dried with caution prior to weighing; other reagents were analyzed gravimetrically for volatile components, and then used in air-dry form. The synthesis was performed in two steps. Firstly, LSb_2O_6 (L = Mg, Co, Ni, Cu, Zn) antimonates were prepared at 1373 K in air. After verifying their formation by X-ray diffraction (XRD), these phases were reacted with appropriate amounts of K_2CO_3 and divalent metal-containing reagent. Potassium carbonate was added in empirically chosen excess (3–10%) to compensate for volatilization of K_2O at high temperatures. Reagents (2–4 g) were carefully mixed, pressed into pellets to enhance component interdiffusion, placed in a packing powder of the same composition to reduce potassium volatilization and exclude contact with crucible, fired and then reground. This procedure was repeated 3–5 times. The temperature of the initial firing steps was 1023 K for carbonate-containing mixtures and 573 K when nickel acetate was used. Solid-state reactions at 1223–1473 K were followed by quenching onto a massive steel plate to prevent phase changes. The obtained samples were kept in a glass container with fresh desiccant to avoid water uptake from the atmosphere. Phase relations and cell parameters of magnesium and cobalt-containing phases were characterized by XRD using a DRON-2.0 diffractometer (Ni-filtered Cu$K\alpha$ radiation). The XRD patterns of anhydrous potassium nickel antimonates were taken using a vacuum chamber on a Philips X'Pert MPD diffractometer (Cu$K\alpha$ radiation, graphite monochromator, $2\theta = 8°$–$140°$, step 0.02°, 8 s/step). To ensure the absence of the traces of absorbed water, the specimens were dried in vacuum at 423 K for 0.5 h prior to the XRD data collection. A Rigaku D/Max/B (Cu$K\alpha$ radiation, graphite monochromator) instrument with a similar scan mode was used to collect X-ray data of samples equilibrated under ambient conditions. The crystal structures of anhydrous phases and the unit cell parameters of the hydrates were refined using the Fullprof program [19]. Thermogravimetric and differential thermal analyses (TG/DTA) were performed using a SETARAM TG-DTA LabSys instrument. Ceramic samples for the total conductivity measurements were prepared from pre-calcined powders by uniaxial hot pressing (1373 K, 40 MPa). One cylinder-shaped green compact (ca. 11 mm in diameter, 6–7 mm thick) was placed into a hot-pressing die and surrounded with coarse-grained alumina to ensure the quasi-hydrostatic regime. After pressing, bar-shaped samples of approximate size $10 \times 3 \times 4\,mm^3$ were cut and polished. The density of the samples was about 80% of theoretical. Only single-phase ceramics, characterized by XRD prior to the electrical measurements, were used for the impedance spectroscopy studies carried out in the frequency range 20 Hz–1 MHz (Hewlett-Packard 4284A LCR meter, Pt electrodes). The measurements were performed in dry and humidified air at partial water vapor pressures up to 60 kPa.

3. Results and discussion

3.1. Compound formation in the systems K_2O–LO–Sb_2O_5 ($L = Ni^{2+}$, Mg^{2+}, Co^{2+}, Cu^{2+}, Zn^{2+})

For possible formation of the structures based on the brucite-like layers, the joins with (L + Sb)/O ratio of 1:2 are of main interest in the composition triangles. The achievement of phase equilibrium in these systems is complicated due to (i) low reactivity of LO oxides, in contrast to that of highly acidic Sb_2O_5 and basic K_2CO_3, (ii) volatility of K_2O at elevated temperatures, and (iii) instability of Sb(V) at the antimony-rich corner. The studies on phase relations were thus limited to the joins shown in Fig. 1; the first two limitations were overcome by the use of a two-stage synthesis approach, adding potassium excess and using a packing powder in the course of synthesis. The prepared compositions (Fig. 1) may be expressed by the general formula $K_xL_{(1+x)/3}Sb_{(2-x)/3}O_2$. Since tetragonal hollandite-type (H) phases are known to exist at $x = 0.17-0.25$ [20,21], the present work was focused on the compositions with x values from 0.5 to 1.0.

Indeed, several new layered phases with L = Ni, Mg and Co were identified in the mentioned composition ranges (Fig. 1). Their powder XRD patterns were indexed using hexagonal unit cells, with lattice constants and relative intensities characteristic of the P2 or P3 types (Table 1). Despite similar ionic radii, no brucite-related compounds were found for L = Cu or Zn; the samples consisted mostly of $KSbO_3$ and LO with minor amounts of unidentified phases. The most obvious

reason for such a difference relates to the coordination preferences of L^{2+} cations. Ni^{2+}, Mg^{2+} and Co^{2+} are stabilized in octahedral environment and thus easily mix with Sb^{5+} in the brucite-like layers, whereas Zn^{2+} prefers tetrahedral coordination and Cu^{2+} is known to adopt square (bi)pyramidal or square planar coordination due to the Jahn–Teller effect. One should also note that cobalt-containing phases exhibit a decrease of the lattice parameter **a**, governed by the (Co,Sb)–O distance, when cobalt content increases (Table 1). This suggests an appearance of Co^{3+} in the structure.

In contrast to Na_2O–LO–Sb_2O_5 systems [18], no O3-type phases were observed in the title systems, similar to K_2O–LO–SnO_2 [7]. Only phases with prismatic coordination of K^+ were found, although the prisms in ionic compounds are less stable than octahedra due to shorter O–O distances. This fact confirms the hypothesis [12] that the preference to form P2 or P3 structures rather than O3 is due to the repulsion between the alkali cations. Small size of higher-valence cations dictates short **a** axis lengths, i.e., 2.94–3.00 Å for titanates [9–16], 3.05–3.08 Å for antimonates ([18] and Table 1), and 3.11–3.25 for stannates [6,7]. In the O3 structure, each cation has six neighbors at distances equal to the **a** parameter, which should result in a strong K–K repulsion destabilizing the lattice. The K–K distances may be increased in cation-deficient P2 or P3 structures due to redistribution of the potassium ions over a great number of geometrically equivalent prisms. This is, however, impossible in the O3 structure with small tetrahedral interstices, less suitable for large potassium cations. For smaller sodium ions, the Na–Na distances of 3.05–3.25 Å are quite common. Hence, only O3 phases were found in Sb-containing systems [18], whereas the Na_2O–LO_x–TiO_2 systems with shorter *a* axes contain both the O3 and P2 structures [9–16].

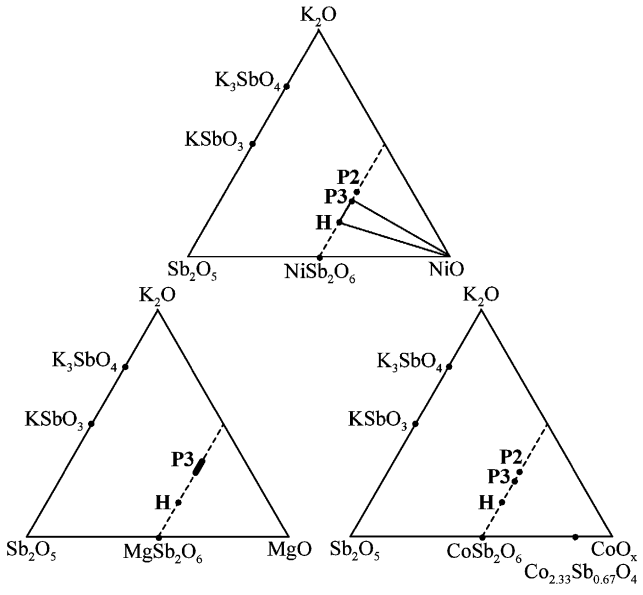

Fig. 1. Composition triangles illustrating compound formation in K_2O–LO–Sb_2O_5 (L = Mg, Ni, Co) systems at 1223–1473 K. Hollandite-type phases are marked with symbols H. P3 and P2 indicate phases with the structures based on brucite-like layers.

Similar to stannate systems [7], the P3-type antimonates form at x values lower than that for P2 (Fig. 1, Table 1). Single-phase P2-type composition, $K_{0.56}Ni_{0.52}Sb_{0.48}O_2$, was obtained at 1373–1473 K. The powder of P3-type $K_{0.5}Ni_{0.5}Sb_{0.5}O_2$, synthesized at 1223 K, contained traces (less than 3%) of P2 phase, $NiSb_2O_6$ and, probably, NiO; firing of the same sample at higher temperatures resulted in a mixture of P3 and P2 phases, with the amount of the latter increasing with temperature. Attempts to employ compositions with lower or higher potassium content than mentioned above, led to the formation of mixtures of layered phases with $NiSb_2O_6$ and/or NiO; at $x = 0.5-0.56$, a mixture of P2 and P3-type phases formed at 1223–1473 K. $K_{0.59}Mg_{0.53}Sb_{0.47}O_2$ composition of P3 type was synthesized at 1373 K; the P2-type phase was not observed in the Mg-containing system perhaps due to the higher formation temperature. Taking into account that one important factor enhancing alkali ion mobility is a low ionicity of L–O bonds and, hence, high electronegativity of M^{2+} [17], the Ni-containing phases were selected for detailed studies as most promising. However, attempts to prepare nickel-containing P3-type ceramics were unsuccessful due to extremely high hygroscopicity of $K_{0.5}Ni_{0.5}Sb_{0.5}O_2$ phase, discussed below. After hot pressing at 1223 K, such ceramics were degraded by atmospheric moisture within an hour. In order to evaluate the electrical properties of P3-type antimonates, the Mg-containing phase, $K_{0.59}Mg_{0.53}Sb_{0.47}O_2$,

Table 1
Compositions and hexagonal cell parameters of new layered phases

Composition	Structure type	Lattice type	Anhydrous		Hydrated	
			a (Å)	*c* (Å)	*a* (Å)	*c* (Å)
$K_{0.59}(Mg_{0.53}Sb_{0.47})O_2$	P3	Rhombohedral	—	—	3.080(4)	21.00(4)
$K_{0.5}(Ni_{0.5}Sb_{0.5})O_2$	P3	Rhombohedral	3.05303(5)	18.9928(7)	3.0601(3)	21.026(2)
$K_{0.56}(Ni_{0.52}Sb_{0.48})O_2$	P2	Hexagonal primitive	3.05477(2)	12.6271(2)	3.0620(1)	14.093(1)
$K_{0.5}(Co_{0.5}Sb_{0.5})O_2$	P3	Rhombohedral	—	—	3.08(1)	20.60(6)
$K_{0.86}(Co_{0.62}Sb_{0.38})O_2$	P2	Hexagonal primitive	3.05(1)	12.81(3)	—	—

was therefore selected for the conductivity studies; for P2 type, $K_{0.56}Ni_{0.52}Sb_{0.48}O_2$ was tested.

3.2. Crystal structure of potassium nickel antimonates

XRD patterns of the new potassium nickel antimonates, $K_{0.56}Ni_{0.52}Sb_{0.48}O_2$ and $K_{0.5}Ni_{0.5}Sb_{0.5}O_2$, were indexed using hexagonal unit cells; then, taking into account systematic absences and relative intensities, the P2 and P3 structures were proposed for these phases. Tables 2–4 and Figs. 2 and 3 present results of Rietveld refinement for both materials; the achieved fit quality confirmed that $K_{0.56}Ni_{0.52}Sb_{0.48}O_2$ and $K_{0.5}Ni_{0.5}Sb_{0.5}O_2$ belong to the P2 and P3 structural types, respectively. The polyhedral representation of refined crystal structures is given in Fig. 4. Both lattices contain $(L,M)O_{6/3}$ layers with different orientations to each other. The absence of superlattice lines indicates that there is no long-range Ni/Sb ordering, although a short-range order should exist according to the bond valence principle. It is important to note that gliding of $(L,M)O_{6/3}$ sheets may lead to the change of P3-type structure to O3-type, while P3→P2 transition via this mechanism is impossible. Thus, the high-temperature transformation of $K_{0.5}Ni_{0.5}Sb_{0.5}O_2$ from almost pure P3 to the P3–P2 phase mixture should involve reconstruction rather than simple gliding.

In both P2 and P3 lattices, K^+ cations have trigonal prismatic coordination, with one type of prisms in P3 structure and two types in P2 (Fig. 4). In the latter case, one type of prism shares two basal faces with $(L,M)O_6$ octahedra; other prisms share faces with empty tetrahedra. The P3 structure comprises prisms sharing one triangular face with an occupied octahedron and another face with a tetrahedral hole. Table 3 presents atomic coordinates, site occupancies and isotropic thermal parameters obtained from Rietveld structure refinement. Attempts to refine site occupancies led to charge unbalance and did not improve the fit significantly. The occupancies were thus fixed according to the charge-balanced $K_xNi_{(1+x)/3}Sb_{(2-x)/3}O_2$ formula, i.e., assuming no vacancies in the rigid brucite-like layers. The Ni/Sb ratios were taken from the starting compositions. Based on the sensitivity of the X-ray phase analysis for NiO, $KSbO_3$ or other potential impurities, the estimated error of Ni/Sb ratios does not exceed 0.02, this is not greater than the expected uncertainty of occupancy refinements. Only occupancies of K1 and K2 sites in P2 were refined (with their sum fixed to 0.56). Placing potassium atoms to higher-multiplicity positions led to instability of the refinement process and/or negative isotropic displacement parameters. As might be expected, the results show slightly higher alkali site occupancy for prisms sharing triangular faces with tetrahedral holes in the P2 lattice, which is due to K-(L,M) cation repulsion. Notice that the isotropic displacement parameters for K^+ are much higher than for other atoms, in accordance with high potassium mobility. The refinement also showed preferred orientation of platelet grains along (00l) crystallographic planes and significant anisotropic strain broadening.

Table 2
Crystallographic data, XRD data collection and Rietveld refinement details of potassium nickel antimonates

Composition	$K_{0.56}(Ni_{0.52}Sb_{0.48})O_2$	$K_{0.5}(Ni_{0.5}Sb_{0.5})O_2$
Structure type	P2	P3
Crystal system	Hexagonal	Trigonal
Space group	$P6_3/mmc$ (no. 194)	$R-3m$ (no. 166)
Unit cell dimensions (Å)	$a = 3.05477(2)$	$A = 3.05303(5)$
	$c = 12.6271(2)$	$C = 18.9928(7)$
Cell volume (Å^3)	102.045(3)	153.313(9)
Z (formula units per cell)	2	3
Theoretical density (g/cm^3)	4.649	4.607
2θ range (deg)	8–140	8–140
Number of data points	6600	6600
Number of reflections	60	57
Number of parameters	16	17
Agreement factors		
R_p (%)	9.5	8.9
R_{wp} (%)	12.3	11.2
R(Bragg) (%)	13.4	8.0
χ^2	2.64	2.65

Table 3
Atomic coordinates and thermal parameters for the crystal structures of potassium nickel antimonates

	Wyckoff position	Occupancy	x	y	z	U_{iso} (Å^2)
$K_{0.56}(Ni_{0.52}Sb_{0.48})O_2$ ($P2$ type)						
K1	2d	0.284(3)	2/3	1/3	1/4	0.032(2)
K2	2b	0.276(3)	0	0	1/4	$= U_{iso}$(K1)
Ni	2a	0.52(−)	0	0	0	0.0019(2)
Sb	2a	0.48(−)	0	0	0	$= U_{iso}$(Ni)
O	4f	1(−)	1/3	2/3	0.0837(4)	0.0021(9)
$K_{0.5}(Ni_{0.5}Sb_{0.5})O_2$ ($P3$ type)						
K	6c	0.25(−)	0	0	0.1639(5)	0.031(2)
Ni	3a	0.5(−)	0	0	0	0.0037(2)
Sb	3a	0.5(−)	0	0	0	$= U_{iso}$(Ni)
O	6c	1(−)	1/3	2/3	0.0559(2)	0.0042(9)

Table 4
Selected interatomic distances and angles for the crystal structures of potassium nickel antimonates (Å)

$K_{0.56}Ni_{0.52}Sb_{0.48}O_2$ (P2 type)		$K_{0.5}Ni_{0.5}Sb_{0.5}O_2$ (P3 type)	
(Ni,Sb)–O × 6	2.056(2)	(Ni,Sb)–O × 6	2.058(2) Å
K1–O × 6	2.743(4)	K–O × 3	2.735(6) Å
K2–O × 6	= K1–O	K–O × 3	2.754(6) Å
(Ni,Sb)–O–(Ni,Sb)	95.96(15)°	(Ni,Sb)–O–(Ni,Sb)	95.87(13)°

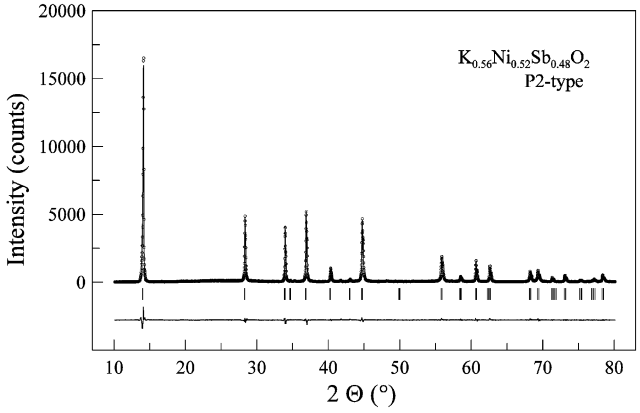

Fig. 2. Observed, calculated and difference XRD patterns of the $K_{0.56}Ni_{0.52}Sb_{0.48}O_2$ (P2) phase in the low-angle region.

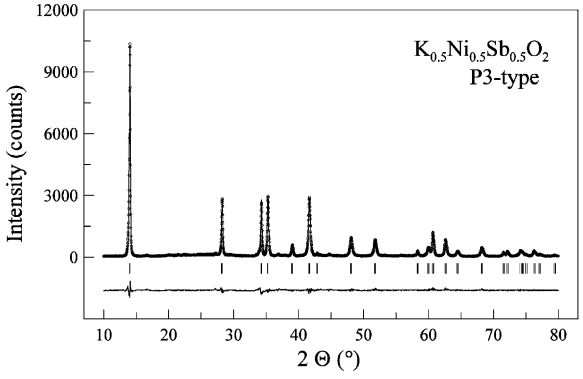

Fig. 3. Observed, calculated and difference XRD patterns of the $K_{0.5}Ni_{0.5}Sb_{0.5}O_2$ (P3) phase in the low-angle region.

Table 4 lists selected interatomic distances and angles for both the P2 and P3 phases. The bond lengths in the octahedra agree with the average ionic radii sum, 2.03 Å [22]. The K–O distances are somewhat larger than the corresponding sum of radii (2.76 Å), which is typical of sites with low occupancy factors [22]. Due to cation–cation repulsion, (Ni,Sb)–O–(Ni,Sb) bond angles are larger than 90°, i.e., the octahedra are flattened along the three-fold axis.

3.3. Electrical conductivity

The impedance spectra obtained for $K_{0.56}Ni_{0.52}Sb_{0.48}O_2$ (P2) and $K_{0.59}Mg_{0.53}Sb_{0.47}O_2$ (P3) ceramics

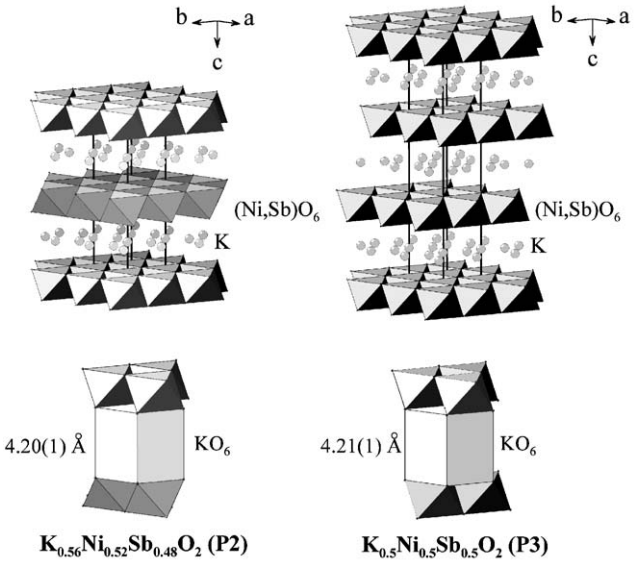

Fig. 4. Polyhedral representation of $K_{0.56}Ni_{0.52}Sb_{0.48}O_2$ (P2) and $K_{0.5}Ni_{0.5}Sb_{0.5}O_2$ (P3) crystal structures.

are typical for solid electrolytes, as illustrated by Fig. 5. At 430–640 K the spectra consist of an arc extrapolating to the origin and a low-frequency "tail" due to the electrode response. At higher temperatures, only the electrode signal with high-frequency intercept, corresponding to the sample resistance, was observed. This type of impedance spectra suggests a dominantly ionic character of the conduction, in agreement with stable oxidation states of Sb(V), Mg(II) and Ni(II), which was confirmed by white and light-green color of the samples, as contrasted with transition metal bronzes.

Fig. 6 compares the temperature dependencies of total conductivity of the title materials and several stannate phases [6,7]. With respect to Sn-containing solid electrolytes such as $K_{0.72}In_{0.72}Sn_{0.28}O_2$ [6], the mixed antimonates exhibit enhanced cation transport properties at temperatures below 400 K. This results from lower activation energy (E_a) of the antimonates, most likely associated with higher K^+ cation deficiency, as for $Na_xNi_{x/2}Ti_{1-x/2}O_2$ ($x = 0.6-1.0$) [9,16]. The difference in the transport properties of $K_{0.56}Ni_{0.52}Sb_{0.48}O_2$ (P2) and $K_{0.59}Mg_{0.53}Sb_{0.47}O_2$ (P3) was found insignificant, which is in agreement with the similar potassium vacancy concentration and hopping distance between potassium sites expressed by the **a** lattice parameter

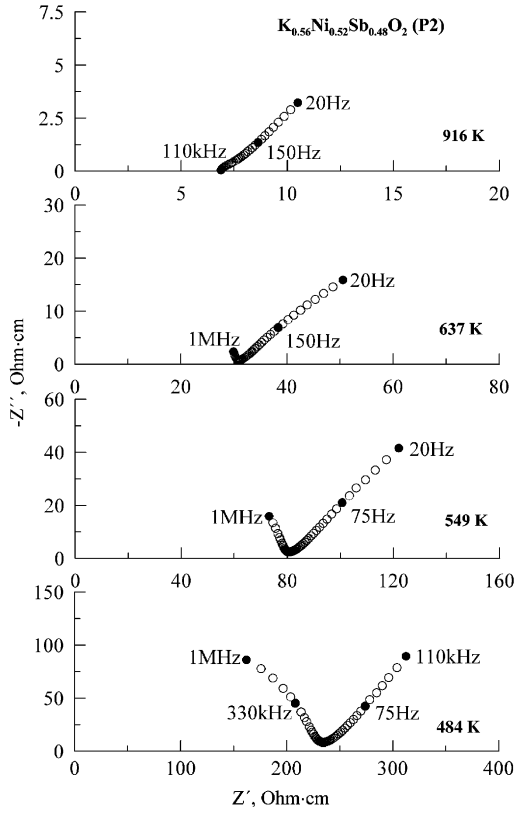

Fig. 5. Typical impedance diagrams of ceramic materials.

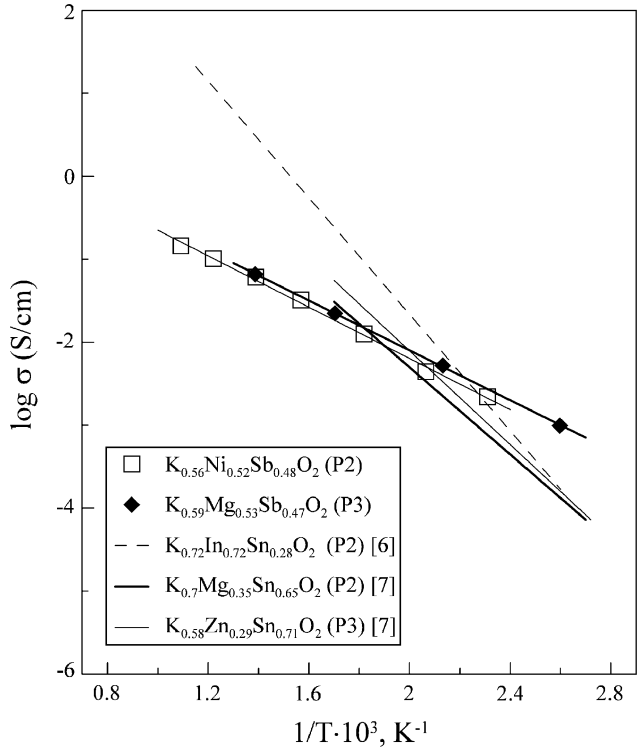

Fig. 6. Total conductivity of $K_{0.56}Ni_{0.52}Sb_{0.48}O_2$ (P2) and $K_{0.59}Mg_{0.53}Sb_{0.47}O_2$ (P3) ceramics in comparison with Sn-containing solid electrolytes [6,7].

(Table 2) in the two structures. Further still, the activation energies for both phases, calculated according to $\sigma T = \sigma_0 \exp(-E_{act}/RT)$, are equal within the limits of experimental error, 35 ± 2 and 33 ± 1 kJ/mol, respectively. The bottleneck size estimated from the crystal structure data for isostructural nickel-containing P3 phase (2.599(3)Å) shows essentially the same value as for P2-type phase (2.597(2)Å).

3.4. Interaction with water vapor: effects on structure and conductivity

During exposure to atmospheric air, the XRD patterns of the layered phases change, indicating an appearance of a second isostructural phase having similar *a* and greater *c* parameters (Fig. 7). The amount of this phase increases with time at the expense of the initial phase. Finally, the initial compound disappears completely, and the powder consists only of the hydrate $K_xL_{(1+x)/3}Sb_{(2-x)/3}O_2 \cdot yH_2O$ formed due to the reaction with atmospheric moisture. The unit cell parameters of hydrated phases (Table 1) show ca. 11% increase in the interlayer distance. The P3-type phases absorb atmospheric water at a much faster rate than P2, which is a result of lower potassium content in the former with essentially the same interlayer spacing. In fact, the initial P3 compounds transformed into the corresponding hydrates in about 1 h, i.e., during the first XRD scan in air. XRD studies of redried powders revealed complete reversibility of the hydration, the initial profile shape being recovered after drying.

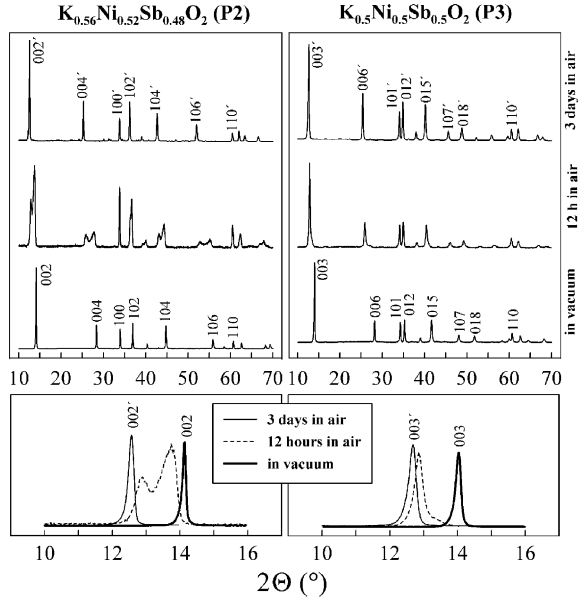

Fig. 7. Hydration of $K_{0.56}Ni_{0.52}Sb_{0.48}O_2$ (P2) and $K_{0.5}Ni_{0.5}Sb_{0.5}O_2$ (P3) phases: evolution of XRD patterns of dried samples in contact with atmospheric air. Reflections of hydrated phases equilibrated with ambient conditions are marked with (′).

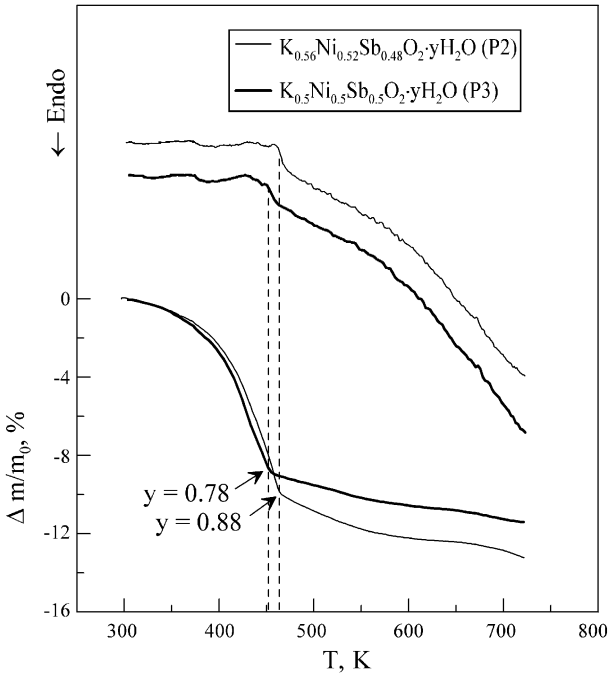

Fig. 8. TG/DTA curves of $K_{0.56}Ni_{0.52}Sb_{0.48}O_2$ and $K_{0.5}Ni_{0.5}Sb_{0.5}O_2$ powders equilibrated in air.

TG/DTA curves (Fig. 8) of the powders equilibrated with ambient air show a significant weight decrease on heating up to 450 K, attributed to the water loss. The water contents calculated from TG data are 0.88 and 0.78 molecules per formula unit for $K_{0.56}Ni_{0.53}Sb_{0.47}O_2$ and $K_{0.5}Ni_{0.5}Sb_{0.5}O_2$ phases, respectively. This corresponds to approximately 1.6 H_2O molecules per K^+ ion for both phases. This behavior is quite similar to the hydration of layered $K_3Sb_3M_2O_{14}$ (M = P, As), which exhibit a reversible H_2O uptake at 300–450 K and absorb about 1.5 H_2O molecules per K^+ ion [23]. A reversible intercalation of water between the brucite-like octahedral layers accompanied by increasing interlayer distance was also reported for P2-type sodium-containing phases, with one H_2O molecule per Na^+ for $Na_{2/3}Co_{1/3}Mn_{2/3}O_2$ [24] or even with four molecules per Na^+ for superconducting bronze $Na_xCoO_2 \cdot 4xD_2O$ [25].

Although the sodium manganite samples [24] were treated with humidified rather than ambient air, the rate of hydration was much slower compared to potassium-containing phases reported in this work. At the same time, Li-containing materials with T2 and O2 structures uptake no water under such treatment [24]. Thus, interaction of the alkali-containing layered phases with humid atmospheres depends on the size of an interlayer alkali cation. Large potassium ions provide greater interlayer distances favorable for water uptake. Further inspection of the XRD pattern, taken after keeping $K_{0.56}Ni_{0.52}Sb_{0.48}O_2$ in ambient air for several days, revealed weak reflections of $KHCO_3$. This indicates that, in addition to the intercalation of water, partial hydrolysis and CO_2 uptake took place, according to the equation:

$$K_xM_{(1+x)/3}Sb_{(2-x)/3}O_2 + (z+y)H_2O + zCO_2 \Leftrightarrow (K_{x-z}H_z)M_{(1+x)/3}Sb_{(2-x)/3}O_2 \cdot yH_2O + zKHCO_3.$$

Hence, the low-temperature regimes of the TG curves (Fig. 8) correspond to the loss of interlayer water (y), whilst weight losses at high temperatures can be attributed to the reaction of layered phases with $KHCO_3$ (or K_2CO_3), resulting in K^+ dissolution in the lattice and losses of CO_2 and remaining H_2O.

The total conductivity of $K_{0.56}Ni_{0.52}Sb_{0.48}O_2$ ceramics was found independent of water vapor partial pressure at 573 K (Fig. 9). At lower temperatures, however, a significant increase in the σ values exhibiting a saturation-like behavior was observed in moist atmospheres. This conductivity increase is obviously due to proton transport, usual in water-containing systems such as oxide hydrates [26–27] and hydrated clays, comprising brucite-like layers [28]. At least two mechanisms of protonic conduction may be supposed:

(i) surface conductivity due to water adsorption, similar to that observed for calcined SnO_2 in humid air [27];
(ii) partial hydrolysis discussed above, which leads to protonation of the layered structure and gives rise to

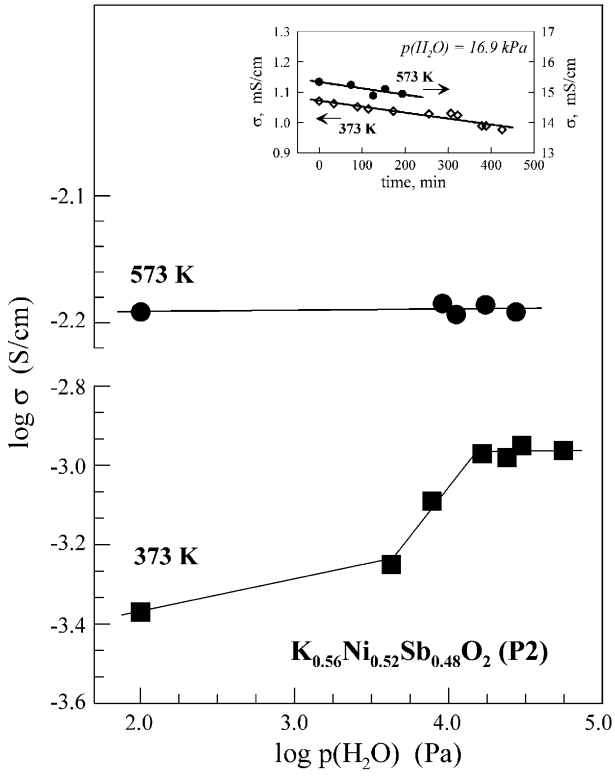

Fig. 9. Dependencies of total conductivity of $K_{0.56}Ni_{0.52}Sb_{0.48}O_2$ ceramics on partial H_2O vapor pressure. Inset shows time dependence of electrical conductivity for the same material exposed to wet air at $p(H_2O) = 16.9$ kPa.

bulk proton conduction; another hydrolysis product should be KOH (which itself is a solid-state proton conductor [29]), and/or its hydrates.

Prolonged exposure to humid air leads to a smooth decrease in the conduction (Fig. 9, inset). Such a behavior is observed even at 573 K, i.e., above dehydration temperature in ambient air (Fig. 8). Since, in wet atmospheres the stability range of the hydrated form should be extended to higher temperatures, one may suggest that water intercalation takes place at elevated temperatures compared to those in air; this may lead to anisotropic expansion of ceramic grains followed by microcracking and a decrease in the conductivity. Indeed, after several cycles in wet atmospheres, cracks were visually observed in the antimonate ceramics.

4. Conclusions

A series of new phases, including $K_{0.59}Mg_{0.53}Sb_{0.47}O_2$, $K_{0.5}Ni_{0.5}Sb_{0.5}O_2$ and $K_{0.5}Co_{0.5}Sb_{0.5}O_2$ having rhombohedral P3-type structure, and $K_{0.56}Ni_{0.52}Sb_{0.48}O_2$ and $K_{0.86}Co_{0.62}Sb_{0.38}O_2$ (hexagonal P2 type) were prepared by the conventional solid-state reaction technique. The crystal structures of $K_{0.5}Ni_{0.5}Sb_{0.5}O_2$ and $K_{0.56}Ni_{0.52}Sb_{0.48}O_2$, refined by the Rietveld method, have space groups $R-3m$ (P3 type) and $P6_3/mmc$ (P2 type) and the unit cell parameters $a = 3.05303(5)$ Å, $c = 18.9928(7)$ Å and $a = 3.05477(2)$ Å, $c = 12.6271(2)$ Å, respectively. Both structure types are based on brucite-like $(L,Sb)O_{6/3}$ sheets with interlayer K^+ ions in the trigonal prismatic coordination. It was confirmed that, similar to other $A_x(L,M)O_2$ systems, the formation of P2 and P3 structure types rather than closely related O3 type is favored by large size of the A^+ cation and short **a** axis lengths of rigid $(L,M)O_{6/3}$ layers. No brucite-related phases are found in $K_x(L,Sb)O_2$ systems where L = Cu or Zn. In contact with atmospheric moisture, a reversible water uptake and consequent formation of hydrates having ca. 11% larger interlayer distances are observed. The impedance spectroscopy studies of P2-type $K_{0.56}Ni_{0.52}Sb_{0.48}O_2$ and P3-type $K_{0.59}Mg_{0.53}Sb_{0.47}O_2$ ceramics suggest a high K^+ cationic conductivity, the values of which at 573 K are 0.016 and 0.021 S/cm, respectively; the corresponding activation energies are 35 ± 2 and 33 ± 1 kJ/mol. The interaction with water vapor results in the higher total conductivity values.

Acknowledgments

The work was partially supported by the Russian Foundation for Basic Research (Grant 00-03-32469), the International Centre for Diffraction Data (Grant-in-aid 00-15), the INTAS (Grant YSF-00-125), and the FCT, Portugal (POCTI program). The authors are grateful to Dr. Rosario Soares for XRD measurements on the Philips X'Pert diffractometer.

References

[1] P. Knauth, H.L. Tuller, J. Am. Ceram. Soc. 85 (2002) 1654–1680.
[2] Y. Miyachi, G. Sakai, K. Shimanoe, N. Yamazoe, Sensors Actuat. B—Chem. 93 (2003) 250–256.
[3] F. Mauvy, E. Siebert, P. Fabry, Talanta 48 (1998) 293–303.
[4] J.M. Paulsen, D. Larcher, J.R. Dahn, J. Electrochem. Soc. 147 (2000) 2862–2867.
[5] C. Fouassier, C. Delmas, P. Hagenmuller, Mater. Res. Bull. 10 (1975) 443–450.
[6] C. Delmas, C. Fouassier, J.-M. Reau, P. Hagenmuller, Mater. Res. Bull. 11 (1976) 1081–1086.
[7] A. Maazaz, C. Delmas, C. Fouassier, J.-M. Reau, P. Hagenmuller, Mater. Res. Bull. 14 (1979) 193–199.
[8] A.F. Reid, J.A. Watts, J. Solid State Chem. 1 (1970) 310.
[9] V.B. Nalbandyan, I.L. Shukaev, Rus. J. Inorg. Chem. 37 (1992) 1231.
[10] I.L. Shukaev, V.A. Volochaev, Rus. J. Inorg. Chem. 40 (1995) 1974.
[11] M.Y. Avdeev, V.B. Nalbandyan, B.S. Medvedev, Inorg. Mater. 33 (1997) 500.
[12] G.V. Shilov, V.B. Nalbandyan, V.A. Volochaev, L.O. Atovmyan, Int. J. Inorg. Mater. 2 (2000) 443.
[13] V.B. Nalbandyan, V.A. Volochaev, I.L. Shukaev, S.M. Pol' shinski, V.I. Sorokin, O.A. Volochaeva, Manuscript deposited by VINITI, No. 3246-B97, 1997, pp. 30–36 (in Russian).
[14] V.A. Volochaev, V.B. Nalbandyan, I.L. Shukaev, O.A. Volochaeva, B.S. Medvedev, In: Materials of the XI Conference on Physical Chemistry and Electrochemistry of Ionic Melts and Solid Electrolytes, Ekaterinburg, vol. II, 1998, p. 62 (in Russian).
[15] Y.-L. Shin, M.-Y. Yi, Solid State Ionics 132 (2000) 131–141.
[16] Y.-L. Shin, M.-H. Park, J.-H. Kwak, H. Namgoong, O.H. Han, Solid State Ionics 150 (2002) 363–372.
[17] P. Hagenmuller, in: R. Metselaar (Ed.), Solid State Chemistry 1982, Elsevier, Amsterdam, 1983, p. 49.
[18] O.A. Smirnova, V.B. Nalbandyan, V.V. Politaev, L.I. Medvedeva, V.A. Volotchaev, I.L. Shukaev, B.S. Medvedev, A.A. Petrenko, in: P. Bezdicka, T. Grygar (Eds.), Solid State Chemistry 2000, Academy of Sciences of the Czech Republic, Prague, 2000, p. 228.
[19] J. Rodriguez-Carvajal, Physica B 192 (1993) 55–69.
[20] G. Bayer, W. Hoffmann, Naturwiss 53 (1966) 381.
[21] A. Pring, J. Smith, D.A. Jefferson, J. Solid State Chem. 46 (1983) 373–381.
[22] R.D. Shannon, Acta Crystallogr. A 32 (1976) 751–767.
[23] A. Lachgar, S. Deniard-Courant, Y. Piffard, J. Solid State Chem. 73 (1988) 572–576.
[24] Zh. Lu, J.R. Dahn, Chem. Mater. 13 (2001) 1252–1257.
[25] J.D. Jorgensen, M. Avdeev, D.G. Hinks, J.C. Burley, S. Short, Phys. Rev. B 68 (2003) 214517.
[26] W.A. England, M.G. Cross, A. Hamnett, P.J. Wiseman, J.B. Goodenough, Solid State Ionics 1 (1980) 231–249.
[27] Yu. Dobrovolsky, L. Leonova, S. Nadkhina, N. Panina, Solid State Ionics 119 (1999) 275–279.
[28] C. Poinsignon, Solid State Ionics 97 (1997) 399–407.
[29] B.Sh. El'kin, Solid State Ionics 37 (1990) 139–148.